Fuel Cell Stack Emulation for Cell and Hardware-in-the-Loop Testing

Peter A. Lindahl, *Member, IEEE*, Steven R. Shaw, *Senior Member, IEEE*, and Steven B. Leeb, *Fellow, IEEE*

***Abstract*— The high costs of fuel cell stacks are often prohibitive for research applications. Instead, researchers tend to either perform tests on individual cells under emulated load conditions, or they use model-based emulated fuel cell stacks to test realistic loads. This paper presents an alternative technique that allows the simultaneous investigation of both cell and hardware. In this technique, an amplifier takes as input the voltage of a reference fuel cell and reproduces the "scaled-up" voltage that would be provided by a stack of similar cells. The output terminals of this simulated stack can be connected to realistic loads, which are series connected with the reference cell to maintain a one-to-one correspondence of cell and load currents. This technique allows the simultaneous investigation of stack/load interactions, stack electrochemical performance characteristics, and stack durability under load. The amplifier electronics are independent of the fuel cell allowing its use with all fuel cell types, e.g., solid oxide fuel cells (SOFCs) or proton exchange membrane fuel cells. We demonstrate the emulator using a single planar SOFC and under several real loads. The data collected reveal good steady-state and dynamic accuracy, and the observed electrical interactions highlight the utility of the emulator in cell and hardware-in-the-loop testing. Ultimately, this technique provides fuel cell system researchers and developers a low-cost, easily implemented tool for rapid assessment of novel fuel cell technologies under real-world loading conditions.**

***Index Terms*— Electrochemical devices, electrochemical impedance spectroscopy (EIS), emulation, energy, energy conversion, fuel cells, renewable energy sources, simulation.**

I. Introduction

FUEL cells are electrochemical devices that convert the chemical energy in hydrogen rich fuel to electricity in an efficient, quiet, and clean manner. Individual fuel cells generate small voltages, on the order of 1 V, and must be combined in series, i.e., "stacked," to increase the voltage to useful levels for an electric load. Because fuel cells are direct energy converters (DECs), their terminals provide a conduit for interaction between the stack's load-side electrical demand and its conversion-side electrochemical/physicochemical processes. If the stack's load profile is excessive and/or dynamic in nature, the load can negatively impact the stack's long-term efficacy by causing degradation to the stack's individual cells [1]–[5]. At the same time, the stack's load profile can also be exploited for monitoring the internal stack and cell operation through "call-and-response" tactics. For example, the current ripple imparted by dc/ac inverters and dc/dc converters can be used to monitor the humidity in proton exchange membrane fuel cells (PEMFCs) [6]–[8] and degradation in SOFCs [9]. Furthermore, given the ability to occasionally customize the stack's load, an electrochemical impedance spectroscopy (EIS) can be used to further characterize fuel cell performance and diagnose problematic operation [10]–[12].

Unfortunately, fuel cell stacks are often cost prohibitive for research applications due to their high material and manufacturing costs as well as the expenses associated with operating and maintaining each stack's complicated balance of plant (BoP) [13]–[15]. Furthermore, commercially available stacks often do not accommodate *in situ* individual cell monitoring, such as EIS or postmortem cell analysis, e.g., scanning electron imaging [16], [17], which can identify degradation mechanisms during and after the stack's lifetime, respectively. As such, researchers tend to perform tests on individual cells under emulated load conditions, i.e., cell-in-the-loop testing [6], [17], [18]. While these tests provide insight toward loading effects and monitoring techniques, they do not provide the ability to test full-scale hardware and controllers, e.g., hybrid-source power managers designed to prevent fuel cell stack degradation [19], [20] or *in situ* sensing systems [19], [21], [22].

To perform hardware-in-the-loop tests, several research groups have developed fuel cell stack emulators based on physical models [23]–[28] or empirical data [29], [30]. These emulators represent low-cost alternatives to real fuel cell stacks. Physical model-based emulators have the advantage of not requiring a fuel cell system for empirical data. Their primary benefit is that they reveal performance parameters related to stack's dynamics, the values of which can be used to refine stack design and control methods. However, a fundamental tradeoff exists between model complexity and accuracy. That is, more complicated models can improve emulator accuracy but at the expense of the emulator's bandwidth due to increased computation time. As such, these emulators typically focus modeling depth on a subset of the stack dynamics.

Empirically derived models feature less computational complexity as reduced parameter models are fit to the measured fuel cell stack performance. However, these emulators still

Manuscript received September 18, 2017; revised January 15, 2018; accepted February 25, 2018. Date of publication March 27, 2018; date of current version August 9, 2018. The Associate Editor coordinating the review process was Dr. Mohamed Abou-Khousa. *(Corresponding author: Peter A. Lindahl.)*

P. A. Lindahl and S. B. Leeb are with the Laboratory for Electromagnetic and Electronic Systems, Massachusetts Institute of Technology, Cambridge, MA 02139 USA (e-mail: lindahl@mit.edu).

S. R. Shaw is with the Department of Electrical and Computer Engineering, Montana State University, Bozeman, MT 59715 USA.

Color versions of one or more of the figures in this paper are available online at http://ieeexplore.ieee.org.

Digital Object Identifier 10.1109/TIM.2018.2814070

require the fuel cell stack data for model development and only reproduce stack behavior consistent with the original test conditions. In either case, while these emulators provide an ability to test hardware, they do not provide the same insight into the load's effects on the fuel cells as do tests involving actual cells with emulated loads.

This paper presents a method for stack emulation which allows for both cell and hardware-in-the-loop stack simulations. Here, the electrical terminal output of the emulator is dictated by that of a reference cell instead of model-predicted or data-driven current and voltage set points. Thus, the emulator can be thought of as an amplifier of the voltage/current relationship of the prototype cell. That is, the voltage gain is related to the number of series connected cells in the simulated stack.

This method offers several advantages. Most notably, it allows the explicit ability to study stack/load interactions and their effects on a fuel cell technology at a lower infrastructure and cost burden than a full stack. Although cell and stack models and model-based emulators can provide parameter values associated with certain dynamics, the reference-based emulator provides a testing facility for data collection of a real fuel cell system in response to dynamic loads. Such data can be used to quantify novel fuel cell technology performance in realistic operating scenarios, develop *in situ* stack monitoring and characterization techniques such as impedance spectroscopy [19], [21], [22], and test power management control methods and hardware required for fuel cell stack and load integration [19], [20]. The method also provides flexibility to emulate multiple fuel cell types and devices. Any fuel cell device, e.g., SOFC or PEMFC, can be used as the input to the reference-based system.

The novelty of this paper lies in the development of a scalable and modular cell and hardware-in-the-loop stack simulator useful for rapid fuel cell technology evaluation, and fuel cell stack and load integration. This paper expands on a preliminary emulator design described in [15], with an improved circuit design that makes the emulator more scalable to varying load power requirements. This paper also provides a more extensive description of the emulator dynamics and broader range of emulator performance tests, including its use in powering two real-world power electronic loads.

II. Fuel Cell and Fuel Cell Stack Operation

Fig. 1 depicts a conceptual cross-sectional diagram of an SOFC supplied with reformed hydrocarbon fuel (i.e., the fuel is preconditioned and broken down into simple H_2 and CO constituents) and pure oxygen. The cell itself is a layered structure with a dense ionically conductive electrolyte separating the porous and electrically conductive anode and cathode.

Fuel cells partition the chemical reaction that would occur in ordinary combustion via these layers and an external circuit connecting the load to the cell. Oxygen supplied to the cathode acquires electrons at the cathode–electrolyte boundary. In SOFCs, the resulting oxygen ions diffuse through the electrolyte to the anode–electrolyte boundary where they combine with the fuel constituents and release electrons. These electrons then travel to the cathode through the external

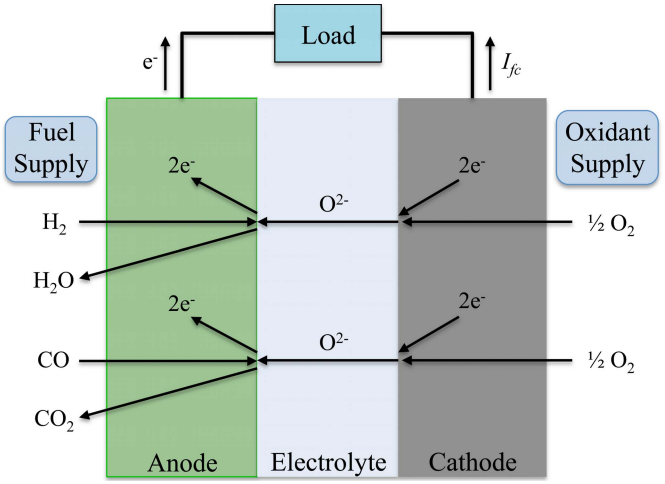

Fig. 1. Conceptual diagram and operation of an SOFC.

circuit, thus providing power to the load and simultaneously completing the circuit and electrochemical reaction. The result of this partitioned process is the direct and efficient conversion of chemical fuel into electricity.

Other fuel cell types feature different partitioning mechanisms. For example, PEMFCs, as their name suggests, feature an electrolyte that conducts hydrogen ions from the anode to the cathode (as such, they cannot facilitate CO as a fuel), but their overall electric terminal behavior is similar.

A single SOFC's output voltage can be described as

$$V_{\text{fc}} = E_{\text{fc}} - V_{\text{fc,act}} - V_{\text{fc,ohm}} - V_{\text{fc,con}} \tag{1}$$

where E_{fc} represents the ideal performance and maximum voltage able to be generated by the fuel cell. It depends on the operating conditions of the cell including its temperature and the supplied fuel and oxidant flow rates and concentrations. As the current through the cell increases due to load demand, polarization losses reduce the effective voltage generated by the cell. These losses, represented in (1) as $V_{\text{fc,act}}$, $V_{\text{fc,ohm}}$, and $V_{\text{fc,con}}$, are overpotential losses due to the electrochemical activation processes, ohmic resistances of cell layers and associated components, and mass transport congestion as reactants and products concentrate under high loads, respectively [13], [14]. In (1), contributions of the various cell layers and components are lumped.

The loss terms of (1) dominate different regions of a cell's current/voltage relationship as depicted in Fig. 2. Fig. 2 provides measured current and voltage data for an H.C. Starck ASC3 anode-supported SOFC with an active area of 18 cm^2. For this test, the cell operated at 750 °C under humidified hydrogen (97% H_2 and 3% H_2O) and humidified oxygen (97% O_2 and 3% H_2O) as fuel and oxidant, respectively.

Under standard operating conditions, a single SOFC generates an electric potential on the order of a volt. To form a power source with convenient output voltages, individual cells are typically "stacked" to generate the combined voltage

$$V_s = \sum_{k=1}^{n} V_{\text{fc},k} \tag{2}$$

where n is the number of series connected cells.

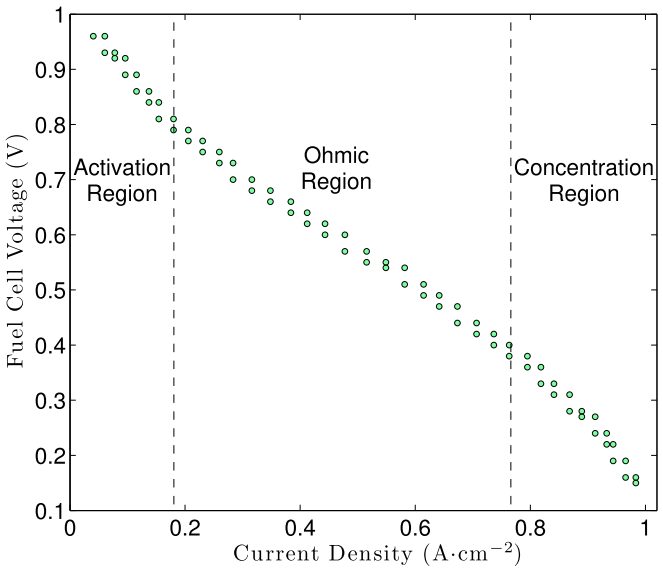

Fig. 2. Measured current/voltage relationship of a typical anode-supported SOFC. (Figure originally published in [15].)

Model-based fuel cell stack emulators [25]–[28] typically assume that each cell is equivalent and operating under consistent conditions, including fuel and oxidant flow rates, reactant partial pressures, and cell temperatures. Under this assumption, their voltages are identical, $V_{\mathrm{fc},k} = V_{\mathrm{fc}}$, and (2) becomes

$$V_s = nV_{\mathrm{fc}}. \tag{3}$$

This assumption, of course, is not always true. Individual cells can differ due to imperfect manufacturing. Furthermore, the fuel cell stack's BoP cannot perfectly ensure identical operation across all cells. For example, a stack's fuel and oxidant distribution and thermal management systems may imperfectly distribute reactants and temperatures, which affect the individual voltages as described in (1).

Still, given adequate BoP operation, sufficient uniformity is usually achievable and justifies (3). For examples, Zhu *et al.* [31] tested 10 Bollard Power System Nexa PEMFC stacks (47 cells and 1200-W power rating) and reported good consistency between cells in each stack. Their worst case stack data revealed a coefficient of percentage variation of $C_v = 3.2\%$. Here, C_v is essentially a percent metric of the standard deviation in the cell voltages defined as [32]

$$C_v = \sqrt{\sum_{k=1}^{n}(V_{\mathrm{fc},k} - \bar{V_{\mathrm{fc}}})}. \tag{4}$$

Corbo *et al.* [32], [33] investigated cell uniformity in 2.6- and 20-kW PEMFC stacks under dynamic loads. They reported C_v values less than 3% except during times of large and fast load dynamics, though the authors also reported that low C_v values could be maintained with a small expense in overall efficiency if air flow to the cathodes was kept slightly elevated.

Similar results have been reported for SOFCs. Burt *et al.* [34], [35] developed a pseudo 2-D planar SOFC stack model to investigate variations between cells in 5, 10, and 20 cell stacks. Their model predicts that cell voltages will vary, particularly at the ends of the stack (i.e., the first few cells and the last few cells), but that the maximum cell–cell voltage variations are only a few percent of the average cell voltage under uniform reactant flows. Yokoo *et al.* [36], [37] built and tested several stacks of anode-supported planar SOFCs ranging in stack height from 1 to 50 cells with the largest stack having a power rating of 1 kW. Their worst case stack test showed a maximum individual cell deviation from the mean cell voltage of less than 5%, while most other tests showed a maximum deviation of less than 2%. Most importantly, for this paper, the maximum voltage deviations between the single SOFC and the average cell voltage for any of the other stacks was approximately 6%.

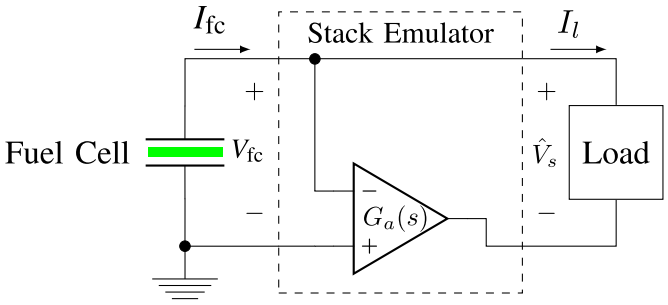

Fig. 3. Conceptual emulator schematic with a single fuel cell for reference.

Thus, for many operating conditions, a fuel cell stack emulator can reproduce the combined *I–V* relationship of an n-cell stack including dynamics with useful accuracy by scaling the operation of a single average cell.

III. Reference-Based Stack Emulation

Fig. 3 shows a schematic of the stack emulation technique. An amplifier with gain $G_a(s)$ reproduces a scaled up and inverted copy of the individual cell's voltage at the negative terminal of the simulated stack, i.e., $\hat{V}_{s-} = -G_a(s)V_{\mathrm{fc}}$. The positive terminal of the simulated stack is connected to that of the fuel cell so that $\hat{V}_{s+} = V_{\mathrm{fc}}$. If the amplifier input has a high impedance, then the reference cell current is virtually identical to the current drawn by the load and the complete electrical relationship between the reference cell and the simulated stack can be described as

$$\hat{V}_s = G(s)V_{\mathrm{fc}} \tag{5}$$

$$I_l = I_{\mathrm{fc}} \tag{6}$$

where $G(s) = G_a(s) + 1$, i.e., the differential voltage gain of the emulator. With a properly designed amplifier, this technique ensures that there is a scaling relationship between the reference cell voltage and the simulated stack voltage over a broad frequency range, while maintaining a one-to-one relationship between the reference cell current and the load current.

The extent to which the emulator reveals the interactions that would occur in a stack of n cells and a load is understood by comparing the block diagrams of Fig. 4. These block diagrams show the transfer function $(I_l/V_{\mathrm{fc},o})$ for an n-cell stack

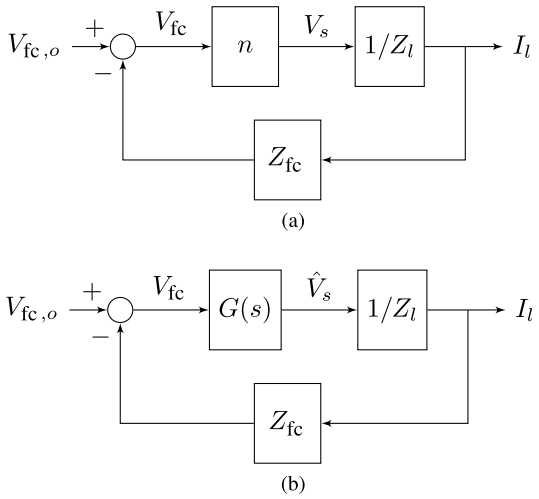

Fig. 4. Block diagrams showing the dynamic operation of a fuel cell stack made of (a) n identical cells and that of (b) simulated fuel cell stack.

[Fig. 4(a)] and for the simulated stack [Fig. 4(b)], and also reveal information on the stability implications of the emulator. Here, the load is modeled as a complex impedance Z_l, and the fuel cell is modeled by its Thevenin equivalent

$$V_{\text{fc}} = V_{\text{fc},o} - I_l Z_{\text{fc}} \tag{7}$$

where $V_{\text{fc},o}$ is the equivalent open circuit voltage of a cell producing voltage V_{fc} at current I_l with a localized complex impedance of Z_{fc}. As illustrated in these diagrams, the salient change in dynamics and gain from the n-cell stack to the simulated stack lies in the emulator's V_{fc} to $\hat{V}_s$ amplification, represented by the $G(s)$ block.

With this configuration, an amplifier design sufficient for a study involving an n-cell simulated stack and a particular load must have:

1) a dc gain and output voltage range sufficient for simulating an n-cell stack;
2) a flat passband with bandwidth exceeding the load frequencies of significance;
3) an ability to sink the maximum current demand of the load;
4) sufficient stability given the characteristics of the fuel cell and those of the load.

One simple and relatively low-cost way to achieve these requirements in an amplifier is to select a power op-amp capable of meeting the first two requirements, and paralleling multiple op-amps in a master–slave configuration to meet the current capacity requirement, as shown in Fig. 5. Regarding the stability requirement, the following analysis elucidates the gain and dynamic implications of an emulator amplifier comprised of paralleled op-amps.

If the open-loop transfer function of the op-amps selected is $A(s)$, then the output voltage of the master op-amp is related to the fuel cell voltage and negative stack terminal voltage as

$$V_{m,o} = -A(s)\left[\frac{R_2}{R_1+R_2}V_{\text{fc}} + \frac{R_1}{R_1+R_2}V_{s,-}\right]. \tag{8}$$

The k slave op-amps, i.e., those configured as unity-gain buffers with feedback resistors, R_f, boost the current capacity

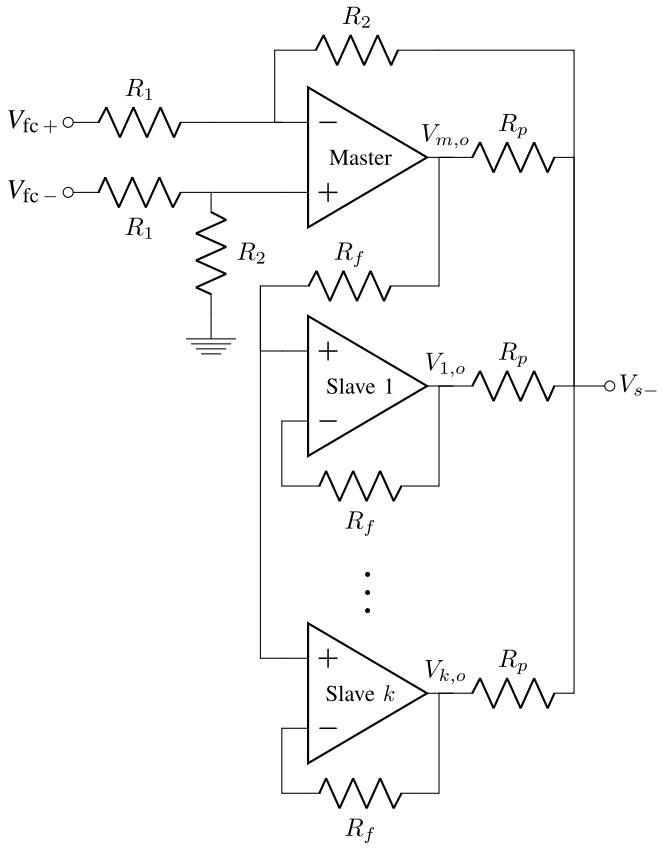

Fig. 5. Schematic emulator with a single fuel cell for reference.

of the amplifier. Their outputs, $V_{1,o}, \ldots V_{k,o}$, are

$$V_{x,o} = \frac{A(s)}{A(s)+1}V_{m,o} \tag{9}$$

for $x = 1 \ldots k$. Resistors, R_p, are low-valued power resistors and allow current sharing between the op-amps. If identical in value, they ensure that the amplifier output is

$$\hat{V}_{s,-} = \frac{1}{k+1}(V_{m,o} + kV_{x,o}). \tag{10}$$

Combining (8)–(10) achieves the transfer function for $G(s)$ as a function of $A(s)$

$$G(s) = \frac{1 + A(s)\left[\frac{A(s)+\frac{1}{k+1}}{A(s)+1}\right]}{1 + \frac{1}{\hat{n}}A(s)\left[\frac{A(s)+\frac{1}{k+1}}{A(s)+1}\right]} \tag{11}$$

where

$$\hat{n} = \frac{R_1+R_2}{R_1}. \tag{12}$$

Typically, $A(s)$ is well modeled by a first-order dominant-pole transfer function,

$$A(s) = \frac{A_0}{\tau s + 1} \tag{13}$$

where A_0 represents the large open-loop dc gain of the op-amp and τ is the time-constant associated with the low-frequency dominant pole. Substituting (13) into (11) and rearranging terms allows $G(s)$ to be written as the second-order transfer

function

$$G(s) = \hat{n}\left[\frac{A_0^2 + A_0\left(1+\frac{1}{k+1}\right)+1}{A_0^2 + A_0\left(\hat{n}+\frac{1}{k+1}\right)+\hat{n}}\right] \times \left[\frac{\frac{\tau^2}{A_0^2+A_0\left(1+\frac{1}{k+1}\right)+1}s^2 + \frac{\left(A_0\left(1+\frac{1}{k+1}\right)+2\right)\tau}{A_0^2+A_0\left(1+\frac{1}{k+1}\right)+1}s+1}{\frac{\hat{n}\tau^2}{A_0^2+A_0\left(\hat{n}+\frac{1}{k+1}\right)+\hat{n}}s^2 + \frac{\left(A_0\left(\hat{n}+\frac{1}{k+1}\right)+2\hat{n}\right)\tau}{A_0^2+A_0\left(\hat{n}+\frac{1}{k+1}\right)+\hat{n}}s+1}\right] \quad (14)$$

where the first term, $\hat{n}$, represents the ideal emulated stack height and is set solely by resistors R_1 and R_2 as previously stated in (12). The terms in the first set of brackets correspond to the dc offset caused by the op-amps' finite gain, A_0. However, so long as $A_0 \gg \hat{n}$, which is true for virtually all practical cases, this offset is ignorable. The terms in the second set of brackets describe the dynamics added to the system by the emulator. Here too, A_0 dominates and $G(s)$ is ultimately very well approximated by the simplified transfer function

$$G(s) \approx \hat{n}\left[\frac{\left(\frac{\tau}{A_0}\right)^2 s^2 + \left(1+\frac{1}{k+1}\right)\frac{\tau}{A_0}s+1}{\hat{n}\left(\frac{\tau}{A_0}\right)^2 s^2 + \left(\hat{n}+\frac{1}{k+1}\right)\frac{\tau}{A_0}s+1}\right]. \quad (15)$$

This transfer function has the effect of a second-order *lag* compensator where the zero and pole locations are functions of the op-amp characteristics, A_0 and τ, the simulated stack height, $\hat{n}$, and the number of paralleled op-amps, $k+1$. If the amplifier consists of only the master op-amp, i.e., $k = 0$, $G(s)$ further reduces to a first-order lag with its single pole at $s = -A_0/(\hat{n}\tau)$ rad/s and zero at $s = -A_0/\tau$ rad/s.

From (15), increasing $\hat{n}$ to emulate a higher cell-height stack increases the dc gain. However, because $\hat{n}$ is present in the denominator and not the numerator, it also shifts the dominant-pole lower in frequency compared to the zeros and nondominant pole locations. Thus, a larger $\hat{n}$ decreases bandwidth and increase the lag's phase shift. Increasing k (adding slave op-amps) causes the zeros of $G(s)$ to form a complex conjugate pair trending toward locations $s = -(A_0/\tau)((1/2)\pm(\sqrt{3}/2)j)$ as k increases. This also slightly increases the amount of phase shift in the lag. Finally, an op-amp with a larger gain-bandwidth product (effectively one with a larger A_0 and/or smaller τ) shifts all the dynamics out in frequency. Collectively, these characteristics of $G(s)$ along with the load impedance, Z_l, and reference cell impedance, Z_{fc}, give insight into emulator effects on accuracy and stability and aid in design if further compensation is required.

IV. Experimental Setup

Fig. 6(a) shows the test fixture used to support a single reference fuel cell during testing. The H. C. Starck ASC3 anode-supported SOFC mounts between two custom designed Inconel 600 platens. These platens serve to support the cell inside an oven, supply the reactant gases to the cell electrodes, and conduct current through the cell as described in Fig. 6(b). Three alumina pins ensure proper alignment of the anode- and cathode-side platens. External to the oven, screws welded to the platen tubes serve as the electric terminals for connecting the emulator circuit, loads, and performing electrical measurements. The humidified hydrogen and oxygen streams are supplied to the anode and cathode platens, respectively, via an MKS gas control system, and an ATS 3210 clam-shell-type oven maintains the cell's temperature at 750 °C during testing.

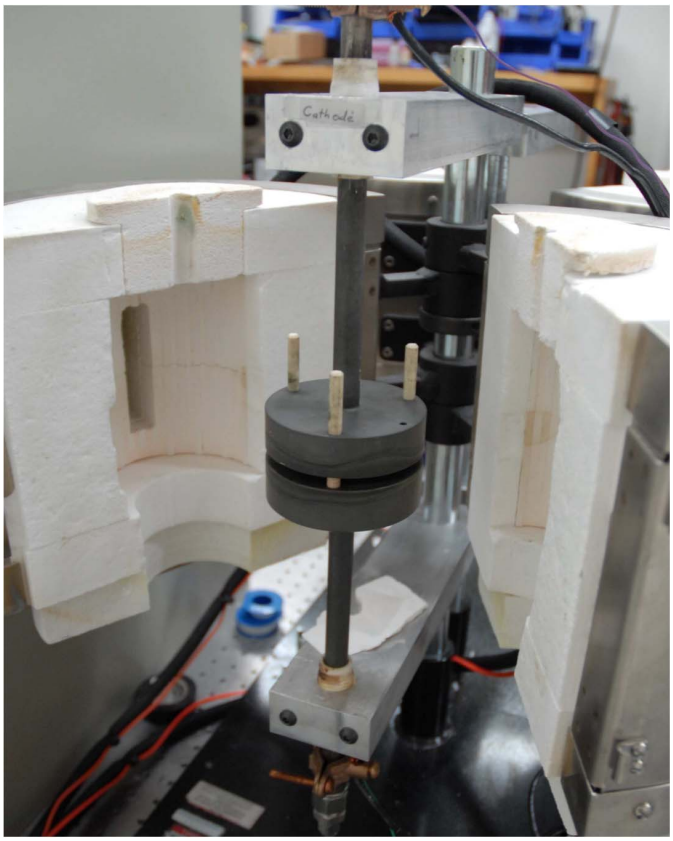

(a)

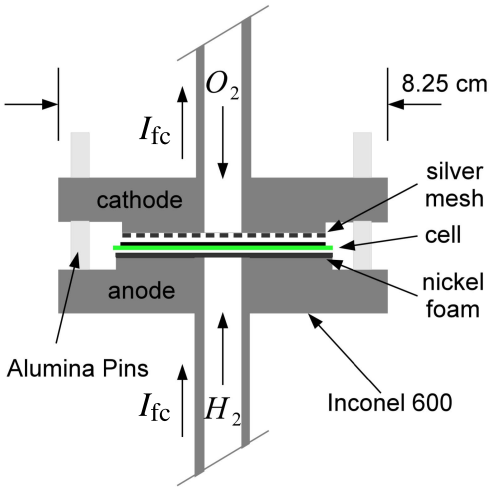

(b)

Fig. 6. Fuel cell test fixture. (a) Fixture in oven. (b) Cross-sectional diagram.

The emulator circuit of Fig. 5 was implemented using four Burr Brown OPA-549 power op-amps. Resistors R_2 and R_1 were chosen to be 19 and 1 kΩ, respectively, to set $\hat{n}$ to

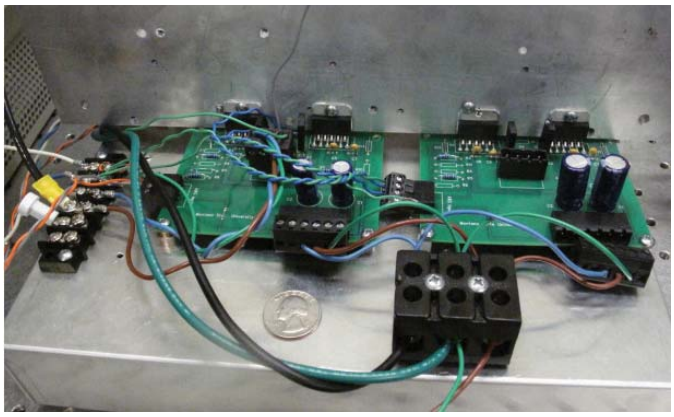

Fig. 7. Circuit implementation of the emulator amplifier used in this paper consisted of four OPA549 power op amps in a master–slave configuration.

correspond to a 20-cell stack. A Xantrex XHR series power supply was used to supply the positive rail, while an HP6012B power supply was used on the negative rail. An image of the emulator circuit is shown in Fig. 7.

To conduct the tests, the cell was first mounted on the Inconel platens. The oven was then programed to increase the temperature to 750 °C at a rate of 3 °C · min^{-1}. Once the oven temperature reached 500 °C, nitrogen was supplied to the anode at a rate of 100 standard cm^3 · min^{-1} (sccm) and oxygen to the cathode at a rate of 30 sccm. Then, once the cell reached the steady-state operating temperature of 750 °C, the nitrogen was slowly replaced by hydrogen at a flow rate of 260 sccm, while the oxygen flow was ramped to 100 sccm. The fuel cell remained in this atmosphere for at least 4 h prior to testing to ensure the anode reduced.

Multiple tests were performed using the fuel cell stack emulator, the conditions of which are summarized in Table I. These included performance characterization tests, including slowly sweeping load current to compare polarization curves of the cell and simulated stack. Also, the EIS data were collected to compare cell and stack dynamics. For demonstrating device and hardware-in-the-loop testing of load/stack electrical interactions, realistic power electronic loads were powered by the emulated stack. These loads included a dc/dc converter powering an automotive bulb and a brushless dc (BLDC) motor turning a propeller.

The current ramp tests and the EIS tests both used an Agilent N3305A programmable load in controlled current mode to vary the load current. The dc/dc converter used was a SynQor NQ60 set to provide a 12-V rail for lighting a Sylvania H6024 incandescent automotive bulb. The BLDC motor tests featured an AXI 5130 motor with an APC 14 × 10 propeller as the mechanical load. The motor controller used was a JETI Spin44 Opto controller. This BLDC motor system is similar to those which might be used in small fuel cell powered unmanned aerial vehicles (see [38], [39]).

For each different test, the cell was brought to operating conditions as described earlier. The load and emulator circuitry were then connected, and the emulator power supplies were turned ON. Measurements of the fuel cell voltage V_{fc}, simulated stack voltage V_s, and current I_l were collected using a National Instruments 9206 16-bit 250-kHz data acquisition module with current measurements obtained with an LEM LA 55-p current transducer.

TABLE I
OPERATING CONDITIONS OF EMULATOR TESTS

All Tests	
H_2 flow rate	260 sccm
O_2 flow rate	100 sccm
Oven temperature	750°C
Polarization Curve Test	
Current ramp rate	0.15 A/s
Maximum load current	15 A
Minimum emulated stack voltage	4 V
Maximum emulated stack power	85 W
BLDC Motor Test	
Propeller speed	55.3 rev/s
Controller MOSFET switching frequency	8 kHz
Average motor current	4.9 A
Average emulated voltage	13.2 V
Average emulated power	65 W
DC/DC Converter Test	
Nominal load current	4 A
Maximum load current	8.3 A
EIS Test	
Average load current	7 A
AC current amplitude	600 mA_{p-p}
Average emulated stack voltage	11 V
Emulated AC stack voltage	0.75 – 1.1 V_{p-p}
Frequency range	100mHz – 1 kHz

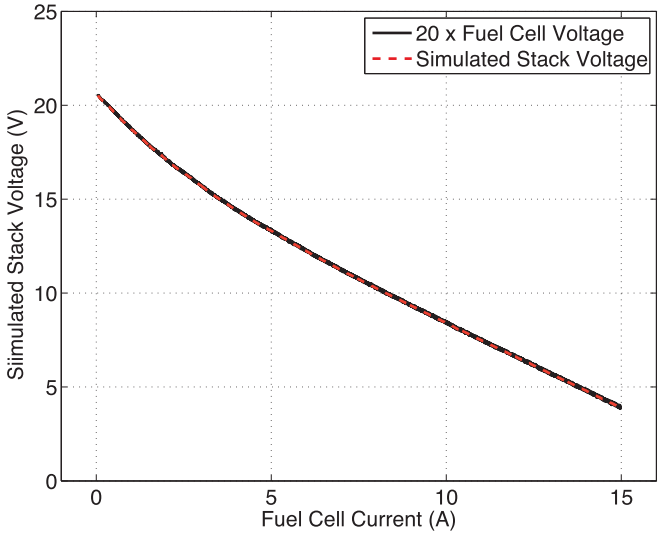

Fig. 8. Measured polarization curve of the simulated stack compared to the measured polarization curve of the reference fuel cell.

V. EXPERIMENTAL RESULTS

Fig. 8 shows a comparison of the measured polarization curves of the single InDEC SOFC cell and the emulated fuel cell stack. The measured fuel cell voltage is multiplied by the ideal n value of 20 for direct comparison to the performance of the simulated stack. The relative agreement of these curves shows the degree to which the emulator scales the cell's output to represent a stack. The stack output voltages are sufficient

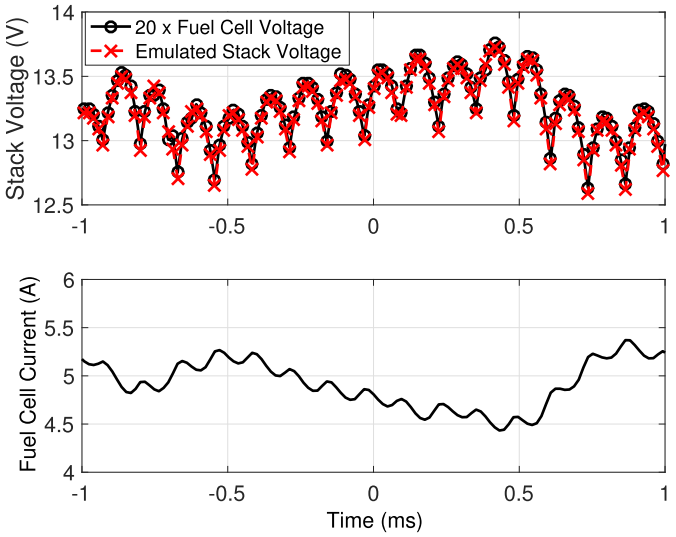

Fig. 9. Current ripple and associated voltage transients of the reference fuel cell and simulated stack under load from an AXI 5330 BLDC motor with a JETI Spin 44-opto motor controller and an APC 14 × 10 propeller.

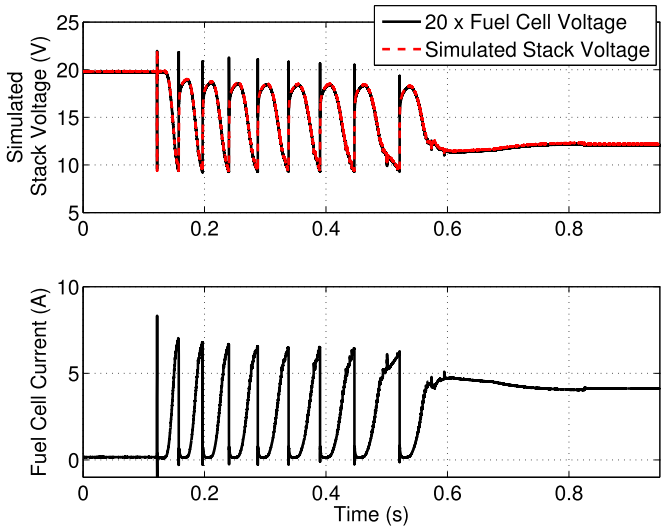

Fig. 10. Turn-ON transient of the reference fuel cell and simulated stack under load of a SynCor dc/dc converter and automotive light bulb.

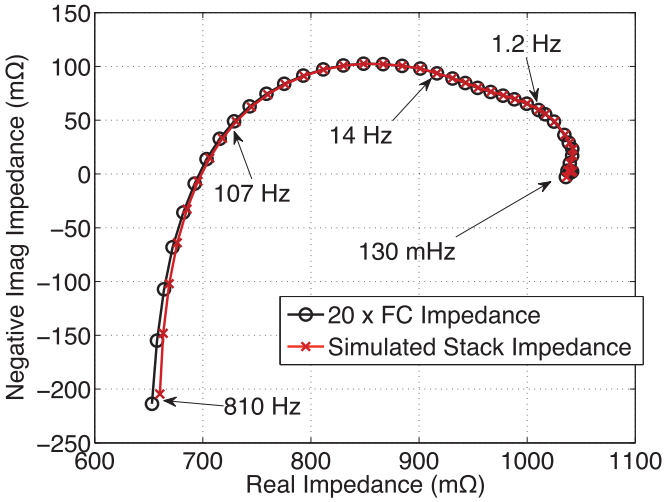

Fig. 11. EIS performed on the reference fuel cell stack emulator.

to test realistic and efficient power electronic topologies and their associated controls. For this test, the current drawn by the electronic load was increased from zero to 15 A at a rate of 0.15 $A \cdot s^{-1}$.

Fig. 9 shows the operation of the emulator and cell while powering an AXI 5330 BLDC motor and APC 14 × 10 propeller load turning at a rate of 55.3 rev/s (3320 RPM). The JETI Spin 44-opto motor controller used to commutate the motor windings also allows control of the motor speed by pulsewidth modulating (PWM) the voltage applied to the motor terminals at a frequency of 8 kHz. As seen on the lower plot, this operation superimposes a small magnitude ripple at the PWM frequency on top of the dc current drawn from the stack. The larger fluctuations in current are induced by the powerful magnets rotating with the spinning rotor. Fig. 9 (top) shows the measured cell voltage and simulated stack voltage response to the current profile. Again, the fuel cell voltage data points are scaled by the n value of 20.

Fig. 10 shows an example of a load and stack connection that produces a surprising interaction. In this case, the load consists of a SynQor dc/dc converter connected to an incandescent light bulb. The plots show the cell and emulator voltages along with the current drawn by the power electronics during a bulb turn-ON transient. Ordinarily, an incandescent bulb connected to a voltage source draws a current spike as the filament heats up to steady state. In this case, the emulator reveals an unstable limit-cycle-type nonlinear interaction. In particular, the in-rush current to the bulb filament causes the voltage on the cell to collapse and the power electronics to under-voltage at roughly nine volts. This process continues for several cycles until the filament is sufficiently hot, after which the bulb functions normally.

Finally, Fig. 11 shows a complex-plane plot comparing the impedance spectroscopy measurements of the reference fuel cell and that of the simulated stack. The impedance measurements are multiplied by the intended stack height, $n = 20$, for comparison with the simulated stack impedance. These results are suggestive of the emulator's ability to facilitate experiments to help link stack electrical output measurements and the inner operating mechanics of the stack. For this test, a logarithmically swept 600-mA peak–peak sinusoid ranging in frequency from 100 mHz to 1 kHz over a period of 175 s was imposed on a dc current of 7 A. The resulting measured current and voltage waveforms were analyzed in MATLAB with their interrelated amplitude and phase determining the small signal impedance of the cell and simulated stack as functions of frequency [40].

VI. Discussion

Figs. 8–11 reveal good performance of the reference emulator in the steady state and under dynamic loading. The polarization curve of Fig. 8 shows the emulator's near-identical matching of the reference cell's steady-state performance characteristics across a broad range of load currents. A maximum load current of 15 A was set as the upper bound, because

beyond this value the op-amps of the reference emulator went into thermal shutdown due to ineffective heat dissipation by the heat sink. This performance could be improved through additional slave op-amps or an active cooling system, e.g., fan-mounted or water-cooled heat sink, so that full quadrant I operation is achievable. Nevertheless, the current system allows operation well beyond the simulated stack maximum power point (around 85 W at 9.6 A).

Figs. 9 and 10 show two examples of the emulator's use for cell and hardware-in-the-loop studies of the electrical interactions between a fuel cell stack and dynamic loads. These types of tests are important, as previous studies of various fuel cell technologies suggest that load/stack interactions are sources of degradation in fuel cell systems [1]–[5]. In the case of the BLDC motor and propeller load (Fig. 9), the fluctuations in the current due to the controller's PWM switching and induction from the motor's rotating magnets result in the corresponding fluctuations in the generated voltages of the prototype cell and simulated stack. Because the current fluctuations have a relatively small magnitude and consist of high-frequency components, the relationship between the current/voltage interaction is dominated by the ionic resistivity of the cell's electrolyte, and the electronic resistivity and inductance of the Inconel platens and connecting cables.

Conversely, in the case of the turn-ON transient of the incandescent bulb powered through the dc/dc converter (Fig. 10), the magnitude of the current draw and the subsequent voltage response is much larger and at a much slower frequency. This leads to a more pronounced, highly nonlinear fluctuation in voltage which is affected by the kinetics of the electrochemical reactions and diffusion rate limitations of the chemical species as well as the ohmic resistances of the cell and platens. The voltage spikes observed in the fuel cell voltage are caused by the abrupt negative step in current and the inductances in the Inconel platens and conductors connecting the cell to the load. These spikes occur on the order of μs and are not followed by the emulator due to slew limit and bandwidth limitations of the op-amps. Thus, the simulated stack voltage does not contain these peaks, which represents a limitation of this particular emulator.

The effects of the stack/load interactions can be diagnosed *in situ* through the EIS analyses like that in Fig. 11. As degradation occurs, the characteristic shape of the complex-plane impedance plot will change as the cell's reaction mechanisms and kinetics are directly related to its impedance dynamics. Fig. 11 indicates the ability of the emulator system to match the scaled impedance of the reference cell, and thus, the emulator's fidelity relative to EIS results and possible applications to *in situ* tests (see [19], [22]).

Extensions of the Emulation Technique: This emulation concept can be extended in a number of useful ways. First, the emulator's application can be extended to a range of direct energy conversion technologies that have inconveniently small potentials, including PEMFCs as well as biological fuel cells, photovoltaic cells, thermoelectric cells, and novel battery technologies. The electronic circuit that comprises the emulator is easily scalable by adding or removing slave op-amps, and is readily modular; numerous op-amps with different characteristics (e.g., rail voltages, gain-bandwidth product, and so on) are commercially available for adapting the concept for different technologies.

Of course, these different unit cell technologies may require unique monitoring and/or control schemes. While these schemes are generally independent of the emulator circuitry, they are nonetheless necessary for realistic stack emulation. For example, PEMFCs require proper humidification of their electrolyte membranes to ensure protonic conductivity, yet excessive liquid water decreases efficiency and eventually starves the membrane of oxygen [41], [42]. To avoid membrane dehydration, input gases are typically humidified to ensure membrane saturation. In laboratory environments, this is often done through gas bubbling [42], i.e., circulating reactants through porous tubes immersed in water, with the water temperature controlling the moisture level. The *in situ* detection of water flooding or membrane drying can be performed via impedance measurement or pressure differentials, and if required, subsequent water removal can be performed by increasing reactant flow rates and/or cell operation temperature [41].

The emulator stack can also be adapted to include the presence of a problem cell by adding a single degraded cell in series with the load. Although this topology cannot easily mimic the fluidic and thermal interactions between a degraded cell and adjacent healthy cells in the stack, it can nevertheless be used to study the impact on the stack's (or portion of the stack's) impedance signature by an unhealthy cell. Furthermore, this setup, while missing the interaction of adjacent cells, can also be used to investigate the effects realistic dynamic loads can have toward failure of "hidden" degraded cells [43]. To that extent, flow rates, temperatures, and other operational conditions can be independently controlled for a second cell to mimic the effects of a single cell under improper BoP operation, though the intercell fluidic and thermal dynamics will still be absent.

Further applications include adding additional cell(s) operating at slightly different temperatures from the reference cell to mimic a full stack's thermal end-effects. There is also no need to restrict the reference fuel cell to be a single cell; a "short" stack could also be used. Importantly, the emulator allows fuel cell system development and fuel cell system integration to be *parallel* as opposed to *sequential* processes. In particular, the complexities of a stack load interactions, as seen in the dc/dc converter result, can be studied and mitigated through power electronic control before or during the development of a stack system.

VII. Conclusion

This paper presents a fuel cell stack emulation technique that accommodates both cell and hardware-in-the-loop studies. The utility of this system is demonstrated by comparing the single cell and emulated stack performance under a variety of loading conditions covering a wide range of load amplitudes and frequencies. Specific cell and hardware-in-the-loop experiments involving the connection of power electronics to the simulated stack provide results that could not be obtained

previously without building or purchasing a fuel cell stack. These results demonstrate the possibility of complex nonlinear interactions between fuel cells and their loads. As such, the emulation technique is highly useful for studying system integration and load management control systems.

REFERENCES

[1] R. S. Gemmen, "Analysis for the effect of inverter ripple current on fuel cell operating condition," *J. Fluids Eng.*, vol. 125, no. 3, pp. 576–585, 2003.

[2] M. Bressel, M. Hilairet, D. Hissel, and B. O. Bouamama, "Remaining useful life prediction and uncertainty quantification of proton exchange membrane fuel cell under variable load," *IEEE Trans. Ind. Electron.*, vol. 63, no. 4, pp. 2569–2577, Apr. 2016.

[3] L. Barelli, G. Bidini, and A. Ottaviano, "Solid oxide fuel cell modelling: Electrochemical performance and thermal management during load-following operation," *Energy*, vol. 115, pp. 107–119, Nov. 2016.

[4] A. Hagen, R. Barfod, P. V. Hendriksen, Y.-L. Liu, and S. Ramousse, "Degradation of anode supported SOFCs as a function of temperature and current load," *J. Electrochem. Soc.*, vol. 153, no. 6, pp. A1165–A1171, 2006.

[5] A. Hagen, P. V. Hendriksen, H. L. Frandsen, K. Thydén, and R. Barfod, "Durability study of SOFCs under cycling current load conditions," *Fuel Cells*, vol. 9, no. 6, pp. 814–822, 2009.

[6] G. Dotelli, R. Ferrero, P. G. Stampino, S. Latorrata, and S. Toscani, "Diagnosis of PEM fuel cell drying and flooding based on power converter ripple," *IEEE Trans. Instrum. Meas.*, vol. 63, no. 10, pp. 2341–2348, Oct. 2014.

[7] G. Dotelli, R. Ferrero, P. G. Stampino, S. Latorrata, and S. Toscani, "PEM fuel cell drying and flooding diagnosis with signals injected by a power converter," *IEEE Trans. Instrum. Meas.*, vol. 64, no. 8, pp. 2064–2071, Aug. 2015.

[8] G. Dotelli, R. Ferrero, P. G. Stampino, S. Latorrata, and S. Toscani, "Low-cost PEM fuel cell diagnosis based on power converter ripple with hysteresis control," *IEEE Trans. Instrum. Meas.*, vol. 64, no. 11, pp. 2900–2907, Nov. 2015.

[9] J. J. Cooley, E. Seger, S. Leeb, and S. R. Shaw, "Characterization of a 5 kw solid oxide fuel cell stack using power electronic excitation," in *Proc. 25th Annu. IEEE Appl. Power Electron. Conf. Expo. (APEC)*, Feb. 2010, pp. 2264–2274.

[10] Q.-A. Huang, R. Hui, B. Wang, and J. Zhang, "A review of AC impedance modeling and validation in SOFC diagnosis," *Electrochimica Acta*, vol. 52, no. 28, pp. 8144–8164, 2007.

[11] S. M. R. Niya and M. Hoorfar, "Study of proton exchange membrane fuel cells using electrochemical impedance spectroscopy technique—A review," *J. Power Sour.*, vol. 240, pp. 281–293, Oct. 2013. [Online]. Available: http://www.sciencedirect.com/science/article/pii/S0378775313006022

[12] X. Yuan, H. Wang, J. C. Sun, and J. Zhang, "AC impedance technique in PEM fuel cell diagnosis—A review," *Int. J. Hydrogen Energy*, vol. 32, no. 17, pp. 4365–4380, 2007.

[13] N. H. Behling, *Fuel Cells: Current Technology Challenges and Future Research Needs*. New York, NY, USA: Elsevier, 2013.

[14] B. Gou, W. K. Na, and B. Diong, *Fuel Cells: Modeling, Control, and Applications*. Boca Raton, FL, USA: CRC Press, 2010.

[15] P. A. Lindahl and S. R. Shaw, "Reference based fuel cell stack simulator," in *Proc. ASME Fuel Cell Sci., Eng. Technol. Conf.*, 2010, pp. 249–255.

[16] F. Bresciani *et al.*, "A combined in-situ and post-mortem investigation on local permanent degradation in a direct methanol fuel cell," *J. Power Sour.*, vol. 306, pp. 49–61, Feb. 2016.

[17] P. A. Lindahl, X. Hu, J. Wold, M. Cornachione, and S. R. Shaw, "Solid oxide fuel cell degradation, recovery and control via the electrical terminals," in *Proc. ASME 12th Int. Conf. Fuel Cell Sci., Eng. Technol.*, 2014, p. V001T06A018.

[18] R. Ferrero, M. Marracci, and B. Tellini, "Single PEM fuel cell analysis for the evaluation of current ripple effects," *IEEE Trans. Instrum. Meas.*, vol. 62, no. 5, pp. 1058–1064, May 2013.

[19] J. J. Cooley *et al.*, "Multiconverter system design for fuel cell buffering and diagnostics under UAV load profiles," *IEEE Trans. Power Electron.*, vol. 29, no. 6, pp. 3232–3244, Jun. 2014.

[20] S.-J. Jang, T.-W. Lee, W.-C. Lee, and C.-Y. Won, "Bi-directional dc-dc converter for fuel cell generation system," in *Proc. IEEE 35th Annu. Power Electron. Specialists Conf.*, vol. 6. Jun. 2004, pp. 4722–4728.

[21] N. Katayama and S. Kogoshi, "Real-time electrochemical impedance diagnosis for fuel cells using a DC–DC converter," *IEEE Trans. Energy Convers.*, vol. 30, no. 2, pp. 707–713, Jun. 2015.

[22] M. Ordonez, M. O. Sonnaillon, J. E. Quaicoe, and M. T. Iqbal, "An embedded frequency response analyzer for fuel cell monitoring and characterization," *IEEE Trans. Ind. Electron.*, vol. 57, no. 6, pp. 1925–1934, Jun. 2010.

[23] N. Benyahia, T. Rekioua, N. Benamrouche, and A. Bousbaine, "Fuel cell emulator for supercapacitor energy storage applications," *Electr. Power Compon. Syst.*, vol. 41, no. 6, pp. 569–585, 2013.

[24] F. Gao, B. Blunier, M. G. Simoes, and A. Miraoui, "PEM fuel cell stack modeling for real-time emulation in hardware-in-the-loop applications," *IEEE Trans. Energy Convers.*, vol. 26, no. 1, pp. 184–194, Mar. 2011.

[25] C. de Beer, P. Barendse, and A. Khan, "Development of an HT PEM fuel cell emulator using a multiphase interleaved DC–DC converter topology," *IEEE Trans. Power Electron.*, vol. 28, no. 3, pp. 1120–1131, Mar. 2013.

[26] G. Marsala, M. Pucci, G. Vitale, M. Cirrincione, and A. Miraoui, "A prototype of a fuel cell PEM emulator based on a buck converter," *Appl. Energy*, vol. 86, no. 10, pp. 2192–2203, 2009.

[27] A. Gebregergis and P. Pillay, "Implementation of fuel cell emulation on DSP and dSPACE controllers in the design of power electronic converters," *IEEE Trans. Ind. Appl.*, vol. 46, no. 1, pp. 285–294, Jan./Feb. 2010.

[28] J.-H. Jung, S. Ahmed, and P. Enjeti, "PEM fuel cell stack model development for real-time simulation applications," *IEEE Trans. Ind. Electron.*, vol. 58, no. 9, pp. 4217–4231, Sep. 2011.

[29] P. Acharya, P. Enjeti, and I. Pitel, "An advanced fuel cell simulator," in *Proc. 19th Annu. IEEE Appl. Power Electron. Conf. Expo. (APEC)*, vol. 3. Feb. 2004, pp. 1554–1558.

[30] V. Boscaino, R. Miceli, and G. Capponi, "MATLAB-based simulator of a 5 kw fuel cell for power electronics design," *Int. J. Hydrogen Energy*, vol. 38, no. 19, pp. 7924–7934, 2013.

[31] W. H. Zhu, R. U. Payne, D. R. Cahela, and B. J. Tatarchuk, "Uniformity analysis at MEA and stack Levels for a Nexa PEM fuel cell system," *J. Power Sour.*, vol. 128, no. 2, pp. 231–238, 2004. [Online]. Available: http://www.sciencedirect.com/science/article/pii/S0378775303009893

[32] P. Corbo, F. Migliardini, and O. Veneri, "Performance investigation of 2.4 kW PEM fuel cell stack in vehicles," *Int. J. Hydrogen Energy*, vol. 32, no. 17, pp. 4340–4349, 2007.

[33] P. Corbo, F. Migliardini, and O. Veneri, "Experimental analysis of a 20 kWe PEM fuel cell system in dynamic conditions representative of automotive applications," *Energy Convers. Manage.*, vol. 49, no. 10, pp. 2688–2697, 2008.

[34] A. C. Burt, I. B. Celik, R. S. Gemmen, and A. V. Smirnov, "A numerical study of cell-to-cell variations in a SOFC stack," *J. Power Sour.*, vol. 126, nos. 1–2, pp. 76–87, 2004.

[35] A. C. Burt, I. B. Celik, R. S. Gemmen, A. V. Smirnov, and W. A. Rogers, "Cell-to-cell variations with increasing SOFC stack size," in *Proc. ASME 2nd Int. Conf. Fuel Cell Sci., Eng. Technol.*, 2004, pp. 31–38.

[36] M. Yokoo *et al.*, "Development of 1 kW class solid oxide fuel cell stack using anode-supported planar cells," *J. Power Sour.*, vol. 184, no. 1, pp. 84–89, 2008.

[37] M. Yokoo *et al.*, "Highly efficient and durable anode-supported SOFC stack with internal manifold structure," *J. Power Sour.*, vol. 178, no. 1, pp. 59–63, 2008.

[38] T. H. Bradley, B. A. Moffitt, D. N. Mavris, and D. E. Parekh, "Development and experimental characterization of a fuel cell powered aircraft," *J. Power Sour.*, vol. 171, no. 2, pp. 793–801, 2007.

[39] P. Lindahl, E. Moog, and S. R. Shaw, "Simulation, design, and validation of an UAV SOFC propulsion system," *IEEE Trans. Aerosp. Electron. Syst.*, vol. 48, no. 3, pp. 2582–2593, Jul. 2012.

[40] P. A. Lindahl, M. A. Cornachione, and S. R. Shaw, "A time-domain least squares approach to electrochemical impedance spectroscopy," *IEEE Trans. Instrum. Meas.*, vol. 61, no. 12, pp. 3303–3311, Dec. 2012.

[41] M. Ji and Z. Wei, "A review of water management in polymer electrolyte membrane fuel cells," *Energies*, vol. 2, no. 4, pp. 1057–1106, 2009.

[42] C. Kunusch, P. Puleston, and M. Mayosky, *Sliding-Mode Control of PEM Fuel Cells*. London, U.K.: Springer, 2012.

[43] A. V. Virkar, "A model for solid oxide fuel cell (SOFC) stack degradation," *J. Power Sour.*, vol. 172, no. 2, pp. 713–724, 2007.

Peter A. Lindahl (S'08–M'15) received the Ph.D. degree in engineering from Montana State University, Bozeman, MT, USA, in 2013.

He is currently a Post-Doctoral Associate with the Research Laboratory of Electronics, Massachusetts Institute of Technology, Cambridge, MA, USA. His current research interests include sensors and instrumentation for energy and power systems, renewable energy generation, and energy policy.

Steven R. Shaw (S'97–M'00–SM'05) received the Ph.D. degree in electrical engineering from the Massachusetts Institute of Technology, Cambridge, MA, USA, in 2000.

He is currently a Professor with the Department of Electrical and Computer Engineering, Montana State University, Bozeman, MT, USA. His current research interests include system identification and controls, energy, and fuel cell systems.

Steven B. Leeb (S'89–M'93–F'07) received the Ph.D. degree from the Massachusetts Institute of Technology (MIT), Cambridge, MA, USA, in 1993.

Since 1993, he has been a Faculty Member with the Department of Electrical Engineering and Computer Science, MIT, where he currently holds a joint appointment with the Department of Mechanical Engineering. His current research interests include the development of signal processing algorithms for energy monitoring and real-time control applications.